Best practices for design and fabrication of biomicrofluidic devices by resin 3D printing

Hannah B. Musgrove, Megan A. Catterton, Rebecca R. Pompano*

Department of Chemistry, University of Virginia. Charlottesville, VA, USA

*Corresponding author, email address rrp2z@virginia.edu

Abstract

Stereolithographic (SL) 3D printing, especially digital light processing (DLP) printing, is a promising rapid fabrication method for bio-microfluidic applications such as clinical tests, lab-on-a-chip devices, and sensor integrated devices. The benefits of 3D printing lead many to believe this fabrication method will accelerate the use of bioanalytical microfluidics, but there are major obstacles to overcome to fully utilize this technology. For commercially available printing materials, this includes challenges in producing prints with the print resolution and mechanical stability required for a particular design, along with cytotoxic components within many SL resins and low optical compatibility for imaging experiments. Potential solutions to these problems are scattered throughout the literature and rarely available in head-to-head comparisons. Therefore, we present here principles for navigation of 3D printing techniques and systematic tests to inform resin selection and optimization of the design and fabrication of SL 3D printed bio-microfluidic devices.

Keywords

digital light processing, stereolithography, SLA, photopolymerizable resins, microfluidic fabrication, cell culture

1. Introduction

In microfluidic device development, a recurring theme is to complete bioanalytical assays at a fraction of the time and cost required for macroscale methods. This aspiration makes rapid and accessible fabrication of microfluidic devices a key goal. Historically, microfluidic fabrication relied heavily on soft lithography methods such as casting polydimethylsiloxane (PDMS) on hard micropatterned masters.[1,2] Soft lithography is primarily a 2D fabrication method, in which multi-layer devices are generated by tedious or challenging manual alignment and bonding. This process is sensitive to any dust that falls onto the layers during aligning and bonding, especially if conducted outside a cleanroom environment. Thus, in order to produce complex 3-dimentional devices monolithically and without a clean room, many groups have turned to 3D printing as a simplified workflow for rapid fabrication in the laboratory.[3–6]

Since the early 2010s, stereolithographic (SL) 3D printing has emerged as a promising technique for fabricating microfluidic devices.[5,7,8] Briefly, this technique works by curing photopolymerizable resins with a UV or visible light source in sequential layers that build on top of one another. Stereolithographic apparatus (SLA) printers were some of the first SL printers and utilize a UV laser guided by mirrors, curing resin point-by-point in a scanning manner in the x and y directions. Direct light processing (DLP) printers were developed later and utilize UV projectors that allow an entire layer to be cured simultaneously from a direct light path. Because of their direct light path, DLP printers tend to have slightly better resolution compared to the similar SLA printers.[5,9] The development of higher resolution DLP printing, along with other SL printers, has increased the use of 3D printing in fields of dentistry, audiology, medicine, and microfabrication.

Compared to traditional fabrication methods, 3D printing reduces cost and fabrication time while increasing product customization.[5,10] Having the ability to readily customize microfluidics also expediates the "fabrication-application-results" process for devices.[1,11] Indeed, many bioanalytical 3D printed devices have been well documented in reviews.[12–15] Applications have ranged widely from bioreactors and probes

made for direct contact with a range of cell lines,[16–19] to approaches that utilized 3D-printed molds to cast microfluidic devices in other materials.[20,21]

When designing 3D printed devices, several compromises must be made, e.g. between resolution and other desirable features, and it is critical to start with the intended application in mind and to understand the limitations of the materials and instrument capabilities before beginning. Limitations for resin 3D printed biomicrofluidics often fall into categories such as inadequate microfluidic feature resolution, mechanical instability (cracks or leaks), material cytotoxicity, or incompatibility of some materials with optical analysis.[22–24] Everything from the resin chemistry and viscosity, to the design and orientation of the print, to environmental factors such as temperature and humidity, can potentially affect the ability to print leak-free devices, small internal microchannels (<1000 μm), or biocompatible, optically-clear devices. Custom, house-made resin formulations may be able to minimize the amount of necessary experimental compromises, though these may not yet be widely available, and rely on individual laboratories having the ability to produce them.[25–27] For commercial resins, resolutions to diminish resin cytotoxicity have started to emerge recently,[28–30] along with solutions addressing print resolution,[26,31–33] imaging compatibility,[25,32,34] and other surface modification and bonding.[35,36] Sifting through this literature for best practices can be challenging for researchers who are new to this rapidly growing field, who would especially benefit from more head-to-head comparisons and a systematic analysis of some of the factors that affect biomicrofluidic design in SL printing.

After working extensively with commercial 3D printers and resins for microfluidics, and learning from the work of pioneering 3D printing laboratories (see citations above), we have converged on a set of strategies to optimize the design and use of a biomicrofluidic part. Here we present a data-supported guide intended to simplify the design and fabrication process for SL 3D printed biomicrofluidic devices for groups that are new to this growing field. We conducted systematic tests of printing and post-treatment conditions designed to optimize the integrity of a printed piece, the resolution of interior channels, and the biocompatibility of the part. This guide follows the order of a typical workflow by first considering resin selection and then

demonstrating how to increase print resolution by using changes in feature design and printer settings. Following printing, cytotoxicity of materials was addressed by demonstrating the extent and effectiveness of post-treating resins for applications involving contact with primary cells. Finally, preparation and considerations for use with fluorescent microscopy is outlined with data displaying autofluorescence and optical clarity of materials. This work is intended to aid in streamlining the adoption of 3D printed devices by more specialized biological research fields and bioanalytical laboratories or those who are new to 3D printing.

2. Materials and Methods

2.1 3D Design and Printing

All printed pieces used for this work were designed either in Autodesk Fusion 360 2020 or Autodesk Inventor 2018 and exported as an .stl file. DWG files of prints shown in figures can be found in the supplementary information. Files were opened in the MiiCraft Utility Version 6.3.0t3 software, where pieces would be converted into sliced files with appropriate layer heights. The files were converted to the correct file format to include settings optimized for either the CADworks3D M50−405 printer (MiiCraft, CADworks3D, Canada), which had a 405 nm light source, or for the CadWorks 3D Printer P110Y, which had a 385 nm source. All prints were printed in one of three resins: FormLabs BioMed Clear V1 (FormLabs, USA), FormLabs Clear V4 resin (FormLabs, USA) or MiiCraft BV007a Clear resin (CADworks3D, Canada).

After printing, all materials were rinsed with isopropyl alcohol using the FormWash from FormLabs, following their wash suggestions.[37] Alternatively, materials were placed in a container with IPA and placed on a rocker for longer periods, extending times by 5 minutes for low viscosity materials and by 1 hour for more viscous resins. Once residual resin was rinsed from the prints, the pieces were dried with compressed

air and post-cured with additional UV dosages using the FormCure (FormLabs, USA). Specific print and post-print settings for each resin and printer can be found in Table S1.

2.2 Viability testing with primary murine lymphocytes

2.2.1 Primary cell preparation

Animal work was approved by the Institutional Animal Care and Use Committee at the University of Virginia under protocol #4042 and was conducted in compliance with guidelines from the University of Virginia Animal Care and Use Committee and the Office of Laboratory Animal Welfare at the National Institutes of Health (United States). Following isoflurane anesthesia and cervical dislocation, spleens were harvested from female and male C57BL/6 mice between 8-12 weeks old. The spleens were collected into complete media consisting of RPMI (Lonza, Walkersville, MD, USA) supplemented with 10% FBS (VWR, Seradigm USDA approved, Radnor, PA, USA), 1× l-glutamine (Gibco Life Technologies, Gaithersburg, MD, USA), 50 U/mL Pen/Strep (Gibco, MD, USA), 50 µM beta-mercaptoethanol (Gibco, MD, USA), 1 mM sodium pyruvate (Hyclone, Logan, UT, USA), 1× non-essential amino acids (Hyclone, UT, USA), and 20 mM HEPES (VWR, PA, USA).

To produce a splenocyte suspension, harvested spleens were crushed through a 70-µm Nylon mesh filter (Thermo Fisher, Pittsburgh, PA, USA) into 10 mL of complete media. The cells were then centrifuged for 5 minutes at 400 xg. The pellet was resuspended into 2 mL of ACK lysis buffer, which consisted of 4.15 g NH_4CL (Sigma-Aldrich, St. Louis, MO, USA), 0.5 g $KHCO_4$ (Sigma, MO, USA), 18.7 g Na_2EDTA (Sigma, MO, USA) into 0.5 L MiliQ H_2O (Millipore Sigma, Burlington, MA, USA). The cells were lysed for 1 minute before being quenched by bringing up the solution to 10 mL with complete media and immediately centrifuging again. The pellet was resuspended into 10 mL of complete media, and density determined by trypan blue exclusion. To prepare for cell culture, the suspensions were diluted with complete media to a concentration of $1x10^6$ cells/mL of media.

2.2.2 Print preparation

Disks with a diameter of 15 mm and a height of 1 mm, designed to fit snugly against the base a 24-well plate, were printed in all three representative resins (BioMed, Clear, and BV007a) following the print settings outlined in Table S1. These pieces were divided into "non-treated," with no further post-treatment, or "treated". The treated prints were further post-treated by soaking in 1x phosphate-buffered saline without calcium and magnesium (PBS, Lot No. 0001018156, Lonza, USA) for 24 hours at 37°C for BV007a or at 50°C (BioMed and Clear resins) mitigate cytotoxicity, with similar treatments shown to be affective in previous works.[38] Both treated and untreated pieces were rinsed again with IPA, dried, and UV sanitized for an additional 10 minutes before use.

2.2.3 Analysis of the viability impact of treated vs. untreated resin

Aliquots of suspended splenocytes (1 mL, 10^6 cells/mL) were added to two 24-well plates containing samples of either treated resins or non-treated resins as previously outlined in section 2.2.1. Wells that did not contain any resins were reserved for plate controls. The cell cultures were incubated for 4 hours at 37°C with 5% CO_2. Following the culture period, the viability of the splenocytes was assessed by flow cytometry using a previously established protocol.[39] Concisely, 500 µL of the cultured samples were stained using Calcein AM (eBioscience, San Diego, CA, USA) at 67 nM in 1x PBS for 20 min at 37°C. The stained samples were centrifuged at 400 xg for 5 min and resuspended in flow buffer (1 x PBS with 2% FBS), after which 4 µL of 1 mg/mL 7-AAD (AAT Bioquest, Sunnyvale, CA, USA) was added. Calcein-AM single stains were prepared using live cells, and 7-AAD single stains were prepared using cells pre-treated for 20 min with 70% ethanol added in a 1:1 v/v ratio to the culture. Additional controls included unstained cells and an ethanol-treated double-stained control. All samples and controls were run on a Guava 4-color cytometer (6-2L) and analyzed with Guava® InCyte™ Software. Live cells were defined as being high in Calcein-AM and low in 7-AAD signal, while dead cells were defined as the inverse.

2.2.4 Analysis of the viability after direct and indirect contact with treated resin

Indirect contact was defined as cell culture in media that had been conditioned by incubation with printed resin, whereas direct contact was defined as cell incubation in physical contact with the printed resins. To test indirect viability, treated BioMed disks were prepared for cell culture as noted in section 2.2.1. Following treatment, the disks were added to a 24-well plate and incubated in complete media for 24 hours at 37°C. After incubation, 1 mL of suspended splenocytes at 10^6 cells per mL were spun down and brought back up in 500 µL of resin-conditioned media. All samples were then cultured for 45 minutes, 4 hours, and 24 hours. Viability was analyzed as in section 2.2.3 to determine the percent of live cells present for each sample.

Direct viability was tested in a similar manner. Treated BioMed disks were added to a 24-well plate, and 1 mL aliquots of suspended splenocytes at 10^6 cells per mL in fresh complete media were added to sample and control wells. Viability was analyzed after 45 minutes, 4 hours, and 24 hours.

2.3 Characterization of material properties of printed pieces

2.3.1 Autoclave compatibility and heat tolerance

To test heat stability of printed pieces, small cubes (5 x 5 x 5 mm) with 1 mm^3 holes through the center were 3D printed in each of the three resin types using settings from Table S1 and autoclaved at 120°C for a 60-minute gravity cycle. Following autoclaving, the pieces were visually evaluated for cracks, delamination, or other alterations to the original design. Following the autoclave test, similar tests were conducted by leaving the prints overnight in ovens at 37°C, 70°C, and 120°C and then visually assessing the prints for discrepancies.

2.3.2 Autofluorescence

Disks with a diameter of 15 mm and a height of 1 mm were printed in each representative resin. A square piece of PDMS was used as a control. All images were collected on a Zeiss AxioZoom macroscope (Carl

Zeiss Microscopy, Germany) with Zeiss filter cube channels including Cy5 (Ex 640/30, Em 690/50, Zeiss filter set #64), Rhodamine (Ex 550/25, Em 605/70, #43), EGFP (Ex 470/40, Em 525/50, #38), and DAPI (Ex ~320-385 nm, Em 445/50, #49). A 500 ms exposure time was used for all images. Following imaging, analysis was performed using Image J v1.530 (imagej.nih.gov). On each image, three 1 x 1 in^2 regions were analyzed for mean gray value in each channel. Background regions were also measured from the borders in each image (outside of the printed parts) and subtracted from each sample measurement individually. The mean gray intensity was calculated for each resin piece and the PDMS control; higher mean gray intensities represented higher autofluorescence of the pieces.

2.3.3 Optical clarity

Disks with a diameter of 15 mm and a height of 5 mm were printed in the FormLabs Clear resin following the print settings listed in Table S1. Several post-processing methods were compared to determine which had the greatest improvement on optical clarity of printed devices. These included printing on glass, a nail polish coating, a resin coating, sanding, and buffing the pieces. A non-processed piece was used as a control, and a glass slide (0.17 mm thick) was used as a benchmark for optimal material clarity.

To prepare the printed-on-glass piece, a print was set up as previously described by Folch, et al.[25] First, small drops of resin were applied to the baseplate using a transfer pipette. A large cover glass with dimensions of 1.42” x 2.36” and a thickness of 0.13-0.17 mm (Ted Pella, Inc. USA) was attached to the baseplate by lightly pressing the slide over the resin then using a UV flashlight to quickly cure the resin between the slide and the baseplate. In the printer software, the initial layer height (“gap height”) was increased by the thickness of the slide (1.7 mm) prior to printing to account for the change in the z-position of the first layer. After printing, the piece was removed from the glass slide with a razor blade and post-cured typically. The glass slide and adherent resin drops were also easily removed with a razor blade.

For acrylate coating, a baseplate-printed piece was coated with generic clear nail polish from a convenience store. The top was coated using the polish applicator, allowed to dry for ~15 minutes, and the process was

repeated on the bottom of the piece. Similarly, a pipette tip was used to apply a thin layer of FormLabs Clear resin to a separate piece on both the top and bottom, with both sides being UV cured for 10 minutes.

For the sanding method, 3M WetorDry Micron Graded Polishing Paper (ZONA, USA) was used. The piece was sanded on both sides starting at a 30 µm grit paper and followed by 15 µm, 9 µm, 3µm, and finally 1 µm grit. Moderate pressure was used to press the piece into the polishing paper in a circular motion to smooth the surface of the piece. Similarly, a generic 4-sided nail buffer (similar products, Walmart, USA) was used to evaluate the impact buffing could have on the printed piece.

Following post-processing, all pieces were imaged to determine optical clarity. All images were collected in the brightfield under transmitted light on a Zeiss AxioZoom macroscope (Carl Zeiss Microscopy). The intensity of light that passed through each piece was measured using Image J for three 1 x 1 inch^2 sections on each image. The average intensity and standard deviation were recorded for n = 3 regions per sample, with the background subtracted from each measurement individually. The relative transmittance, *T*, of each sample was calculated according to Equation 1,

$$T_{relative} = I/I_0 \qquad \textit{Equation 1}$$

where *I* is defined as the average mean gray intensity of the sample, and I_0 is defined as the mean gray intensity of a glass slide. Error was propagated using Equation 2,

$$\delta T = T\sqrt{(\delta I/I)^2 + (\delta I_0/I_0)^2} \qquad \textit{Equation 2}$$

where δ is the standard deviation.

3. Results and Discussion

3.1 Selecting a resin based on predicted resolution, optical clarity, and cytocompatibility

Design of a successful 3D printed bioanalytical tool begins with selection of a suitable resin, a process that currently requires compromises. Ideally, the resins used to 3D print bioanalytical microfluidic devices would be compatible with all cell types, be able to produce milli- and microfluidic sized internal features without mechanical defects and meet imaging requirements of having low background fluorescence and high optical clarity when needed. There has yet to be a commercial resin, however, that integrates all of these ideal properties. Focusing on enhancing one feature (e.g. cytocompatibility) usually results in compromising on another (e.g. print resolution). Because of this, it is useful to understand the key components of resins before choosing a material to work with.

Though specific resin components differ, we found through previous experience that resins in the same category often have similar material properties. For the purpose of bioanalytical microfluidics, the categories investigated in this paper include resins intended to be biocompatible, intended for optical clarity, or designed for the highest microscale resolution. For this work, one test resin from each of these categories was chosen as a case study, and these are listed in Table 1 along with important intrinsic properties. FormLabs BioMed Clear V1 (FormLabs, USA) is considered a biocompatible resin with a USP Class VI biocompatibility rating, where it is approved for contact with live mucosal membranes and skin tissue for >30 days.[40] The FormLabs Clear V4 resin (FormLabs, USA) is representative of a material that offers increased optical clarity. MiiCraft BV007a Clear resin (CADworks3D, Canada) is a low-viscosity resin designed for high print resolution specifically for microfluidic devices.

Table 1: Properties of representative SL resins that inform material choice.

Resin Type	*Biocompatible*	*Optically Clear*	*High Resolution*
Representative resin	FormLabs BioMed	FormLabs Clear	MiiCraft BV007a
Price (USD)*	$349/L	$149/L	$510/kg[†]
% Additives in composition*	<2%	<0.9%	10-15%
Viscosity at RT (mPa•s)*	1350	850-900	75-100
Heat Stability (24h)	120°C, Autoclavable	50°C	37°C

**As of the date of print, all information is currently available from the vendors and material safety data sheets and are relisted here for convenient comparison.*[41–44]

[†] *For BV007a, density is 1.04-1.10 g/mL at room temperature, so 1 kg is ~1 L*

While commercial photocrosslinkable resins for SL printing usually keep their exact compositions as a trade secret, the fundamental chemistry can be found in MSDS documentation. Many SL resins for microfluidics are fairly similar in their basic composition and can be used across different printers, especially with printers that allow for exposure setting adjustments. All three test resins in this work contained monomers and oligomers of an acrylate or methacrylate polymer base, as well as photoinitiators that are activated by UV or violet light from the printer to initiate crosslinking.[41,42,44] Additives were also present, and generally fall into categories of photoabsorbers, dyes, and plasticizers.[45]

Higher concentrations of additives are sometimes used to achieve a large increase in print resolution, e.g. by adding photoabsorbers to reduce the effect of scattered light and/or adding plasticizers to lower the viscosity of the pre-cured resin. MiiCraft's microfluidic BV007a resin, with the highest percent of additives, has a manufacturer-reported viscosity about 10-fold lower than that of the other listed resins (Table 1). Lower viscosity is directly related to a higher print resolution of internal features, as successful generation of hollow printed channels requires that uncured resin easily drains out during both printing and cleaning steps. In highly viscous materials like the BioMed resin, undrained resin is easily retained inside the internal

features, where it may be crosslinked by light that has been transmitted or scattered in excess, especially as subsequent layers of resin are cured above the hollow features.

On the other hand, acrylate monomers, photoinitiators, and plasticizers have all shown cytotoxicity with various cell types, due to factors ranging from oxidative stress to lipophilic reactions with cell membranes.[46–48] Although deliberately leaching these toxic components from post-cured materials can increase cytocompatibility,[30] we have found that in some cases it also decreases material stability, causing cracking or a decrease in material strength and flexibility as the plasticizers are removed. This problem was particularly prevalent with BV007a prints, which peeled apart when leached for longer than 48 hours. For this reason, starting with a more biocompatible material to begin with may better address this problem when working with sensitive cells.[27]

Finally, heat stability can be an important factor for maintaining stable design features during autoclave sanitation or extended handling at physiological temperatures, e.g. for cell culture. We therefore tested the heat stability of each resin (see Methods). The BioMed material was autoclavable and also stable overnight at 120°C, allowing for thorough sterilization should any prints need to be reused or prepped for use with live biomaterials. In contrast, BV007a withstood only mild sanitation procedures through alcohol rinses or UV sanitation, as high heat delaminated the material over time, although it was stable during overnight incubation at 37°C. The Clear resin was found to be intermediate between BioMed and BV007a on most accounts, and we selected it as a standard material for highlighting a typical printing workflow for biomicrofluidics.

3.2 Factors that influence print quality

Material composition has the largest impact on function and printability, but there are several other factors related to instrumentation and environment that have significant impacts on the quality of SL 3D printed pieces (Fig.1). Light sources and exposure settings are close behind material composition in their impact

on resolution due to their effects on the reaction rate and extent of crosslinking, as will be discussed in following sections. Additionally, the material and roughness of the baseplate surface impact both the clarity of the print and how well it remains attached to the baseplate during printing. The orientation of a print as well as its design specifics impact how the print experiences gravitational strain and other mechanical stress. This in turn determines how well internal features and complex designs come off the base plate.

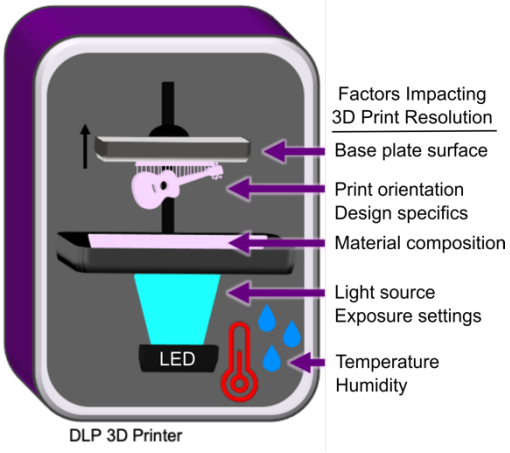

Fig. 1. Schematic of a DLP 3D printer, highlighting the factors of printing that influence print resolution. Digital light processing 3D printers project UV or violet light through optically clear sheets (usually Teflon) into a vat of photopolymerizable resin (pink). In locations where the light is projected, the resin crosslinks to form a solid structure. Exposure and crosslinking are performed layer by layer on the base plate, which lifts up as each concurrent layer is formed. Production of a clean print is dependent on instrumental, environmental, chemical, and design elements that impact either the print surface (base plate), mechanics (print orientation, design specifics), or chemical reaction (material composition, light source, exposure settings, temperature, or humidity).

Humidity and temperature can also impact the how well the photopolymerization reactions take place. Many resins are recommended to be printed at relatively low humidity (20-40%).[49] We have observed that when the humidity increases in warmer months (averaging 45% in the summer in our laboratory, sometimes higher than 50-60%; ~30-35% in winter), print failures become more common: print layers delaminate or base layers do not remain attached to the baseplate. To counteract this, we found that placing a two-way humidity pack (Boveda 49% RH, Boveda Inc., USA) near the resin vat inside the printer helped to regulate the humidity and provide consistency. We also found that increasing the power of the light source by 5-10% partially compensated for humidity increases. Ambient temperature can also influence how well a

material prints as it directly impacts the viscosity of the material and reaction times. This was not explored in depth here, but the typical suggested minimum temperature for printing SL resins is between 20–30°C, with higher temperatures increasing the rate of reaction and improving resolution.[50,51] We and others have found that compensations for temperature changes can be made by increasing exposure time as temperatures decrease, though these may not provide the same structural feature quality, as overcuring is more likely to occur.[50]

3.3 Design and setting considerations for common microfluidic features

In this section, we discuss the role of light exposure and printer settings in controlling print quality, along with design principles for troubleshooting common print failures and improving the resolution of 3D printed microfluidic channels.

3.3.1 Design considerations for wells, cups, or ports

In microfluidic design, particularly for bioassays, wells or cup-like features are often used as reservoirs or ports. If not properly designed, these wells often fall victim to print failure.[52–54] Like other photocrosslinkable polymers, many SL resins shrink a few percent by volume upon crosslinking which may induce mechanical strain.[53,55,56] If the walls of a print are thinner at some points and thicker at others, the thicker regions experience greater shrinkage and may generate defects.[53] Weak structural points can also be formed when thin walls, sharp corners, and sharp edges (~90° angles) are used in a design, and these may not hold up well in the printing process.[57,58] Wells or cup-like features, for example, may experience "cupping," which occurs when hollow features become damaged during printing due to the formation of a pressure differential (Fig. 2). This effect is due to a low pressure region, or suction, formed within the feature as the print is peeled or pulled away from the teflon sheet after each layer is exposed, leading to the cracks and/or holes at weaker structural points in the design as it caves inward under the surrounding pressure (Fig. 2B).[52] Any breaking points may cause leaking when the printed well is later filled with fluid.

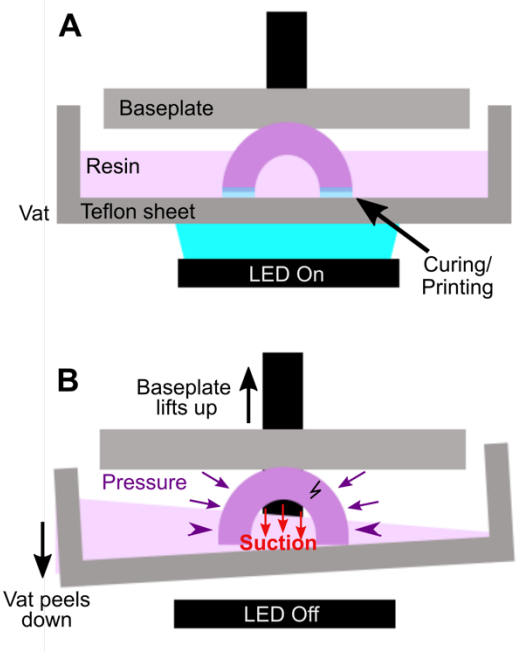

Fig.2. Schematic of "cupping" damage during the printing of a hollow, cup-like feature. (**A**) During printing, a UV light source (LED) forms a new crosslinked layer of resin flush against the teflon sheet. This design is an inverted bowl shape; supports are not shown for clarity. (**B**) After a layer is finished printing, the print is peeled away from the teflon sheet, e.g. by pulling the vat down and/or the baseplate up. This process creates a region of suction within the hollow cup feature; the surrounding pressure, now higher than the pressure within piece, may form a stress fracture on the print.

As a demonstration, a hollow well printed in a square base with 90° square angles and thin walls broke routinely under the pressure build up from cupping and the strain placed on the feature (Fig. 3A). We tested the impact of various strategies to reduce mechanical strain in the design, drawing upon engineering principles.[57,58] The square exterior, with its varied wall thickness around the radially symmetric well, contributes to an uneven stress distribution during resin shrinkage. Increasing the thickness of the base and wall and filleting the connecting edge at the base of the well reduced the risk of cracking the base of the print, but not the appearance of small holes at the base of the well (Fig. 3B). Making the thickness of the walls more uniform around the well-like feature, by rounding the exterior corners of the feature either partially (Fig. 3C) or fully (Fig. 3D) reduced the strain unequal shrinkage as expected, with full rounding producing a well feature with no holes or other leaks.

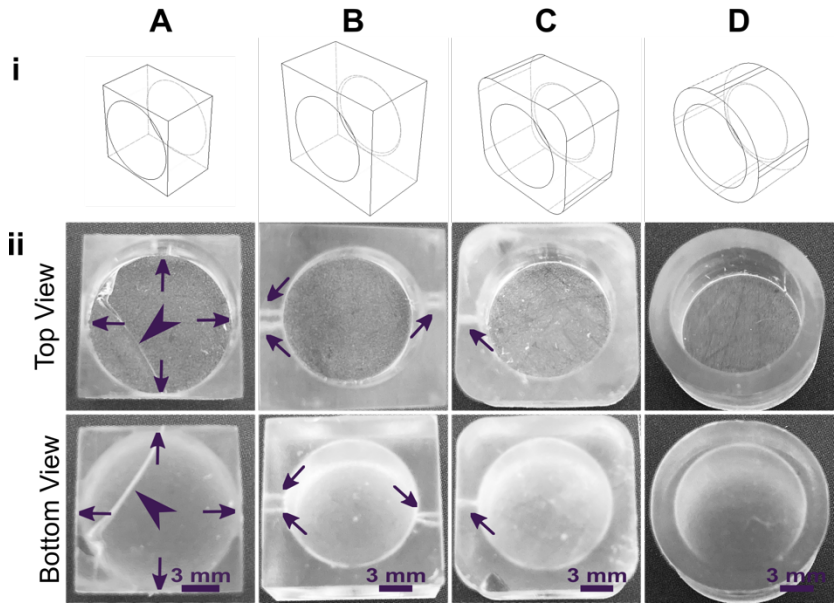

Fig.3. Strengthening the design around well-like features decreases the impacts of cupping and resin shrinkage. (i) Illustrated computer-aid designs, and (ii) photos of the top and bottom views of the corresponding print. All pieces were printed in FormLabs Clear resin. Well **A** had thin walls, thin base, and strain from 90° connections at the bases and the sides. Well **B** had thicker surrounding walls and a thicker, filleted base, but retained 90° outer corners. Wells **C** and **D** further reduced the strain by rounding out the external edges. All pieces were qualitatively evaluated, with the absence of cracks (arrowheads) and pinholes (shown by arrows) indicating a strong design.

3.3.2 Improvement of print resolution of interior features via instrument settings and resin properties

Internal features such as enclosed microchannels are imperative to many 3D printed microfluidic devices. Most commercial resin materials currently yield features at the scale of millimeters or hundreds of micrometers, and it is possible to improve the print resolution of internal features through strategic selection of materials and light sources, and by changing key settings and design aspects.[31] The central requirement is to avoid unintentional crosslinking of uncured resin inside the feature, which would lead to blocked features. Here we tested the extent to which light wavelength, material properties, and layer height influenced the resolution of printed internal features, by determining the smallest channel width that could be printed in a test piece containing six internal channels of decreasing square cross-section (0.2 - 1.2 mm side-length; Fig. 4A).

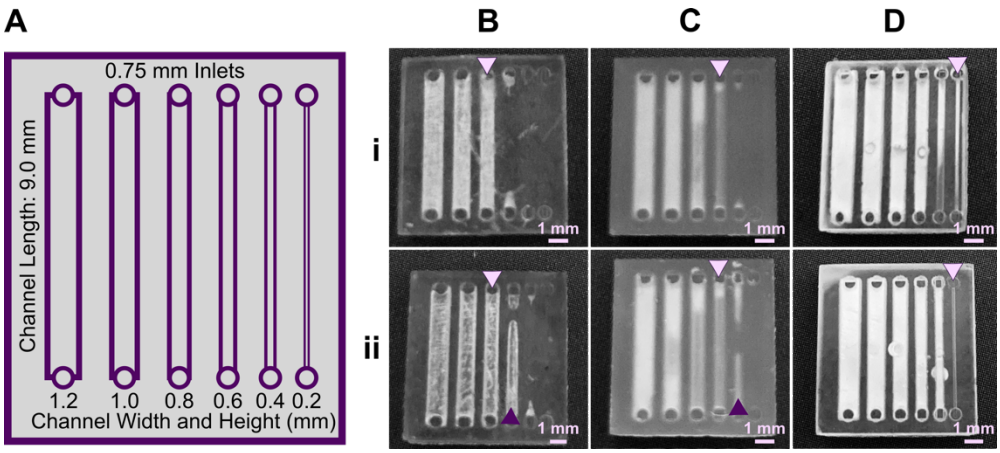

Fig.4. The resolution of internal features can be increased by making changes to the light source, resin viscosity, and print layer height. **(A)** A test piece had six internal channels, 9-mm long with 0.75 mm diameter inlets and varied channel cross-sections as noted. It was printed with **(B-D)** (**i**) 50 µm layer height or **(ii)** 100 µm layer height, as follows: FormLabs Clear resin was printed with a (**B**) 405 nm or (**C**) 385 nm light source; (**D**) for comparison, a low viscosity resin, BV007a, was printed at 385 nm. Other settings were left unchanged, with the exception of increasing exposure times slightly for some 100-µm prints (Table S1). Resolution was determined visually by observing the smallest channel cross-section that could be printed fully (pink arrows) or partially open (purple arrows).

Light sources vary by printer type (laser, LED, or UV lamp) and typically emit at 385 nm or 405 nm. Though most commercial resins can be printed at either wavelength, expediated reactions with higher print resolution occur when the light source best aligns with the excitation peaks of the photoinitiators and absorbers in the material. The impact of wavelength was evaluated by printing test pieces in FL Clear resin, using either a 405-nm or 385-nm printer (Fig. 4B vs 4C). The X,Y-resolution (effective pixel resolution) was similar between the two printers, at 30 and 40 µm for the 405- and 385-nm printers, respectively. In this resin, the crosslinking reaction was more efficient at 385 nm, enabling use of reduced exposure settings (shorter times and/or lower intensities; Table S1), which likely assisted in diminishing bleed-through light allowing uncured resin to drain easier from channels. Consistent with this, channels were printable ~0.2 mm smaller with the 385 nm printer (Fig. 4C) versus the 405 nm source (Fig. 4B).

The need to drain uncured resin out of hollow features during both printing and cleaning means that resin viscosity has a major impact on the resolution of internal features. To demonstrate this, we compared the resolution of FL Clear resin (Fig. 4C) to MC BV007a (Fig. 4D), which have viscosities of ~900 mPa s and ~100 mPa s, respectively (Table 1), using the 385 nm light source. The Clear resin retained uncured resin

in the channels during printing (visible when the device was removed from the printer), and produced open channels only down to 0.6 mm under these conditions. In contrast, no residual BV007a resin was observed in the part prior to rinsing the channels, and the print yielded a resolution of 0.2 mm, the smallest size tested, thus confirming the significant benefit of low viscosity to channel resolution.

Finally, we considered the impact of layer height, which changes the number of layers that must cured directly above hollow features, known as overhang layers. Each overhang layer, though required to close off the top of the feature, is a chance for light to unintentionally penetrate or scatter into the uncured resin that is trapped in the hollow space, potentially crosslinking it. Increasing the layer height reduces the number of overhang layers and works well for designs without strong diagonal features in the z-direction.[59] This setting can be modified on most printers during the file slicing step when converting a design file into a printable file. Using the FL Clear resin, doubling from 50-µm (Fig. 4i) to 100-µm layer height (Fig. 4ii) improved the print resolution of interior channels in the test piece to partially open the next smaller channel (an improvement of <0.2 mm, Fig. 4ii, purple arrows). Therefore, simply decreasing the number of overhang layers decreased the degree of overexposure or bleed-through light and improved print resolution, though not as much as changing from 405 to 385 nm light.

In summary, with its ability to print efficiently at 385 nm and to drain easily with low viscosity, BV007a provided the best print resolution, with 0.2-mm channels printing cleanly at a 50-µm layer height. Printing with the Clear resin, however, nearly achieved 0.4 mm channels if used with a 385 nm light source and 100-µm layer height. While the specifics of printability will change for each design, we found that the light source, material viscosity, and layer height each provide opportunities to increase print resolution of interior microchannels.

3.3.3 Improvement of print resolution of interior features via device design

In addition to light source, materials, and printer settings, there are also design considerations for the microdevice itself that impact internal feature resolution. To demonstrate, we again selected the FL Clear resin due to its higher viscosity and transparency, properties that result in frequent bleed-through curing. We tested the how changes to overhang thickness, addition of draining pores, and changes to channel length impact the print resolution of internal features.

Similar to the effect of layer height during printing, we predicted that design changes intended to reduce the number of UV exposures over hollow features would facilitate drainage of uncured resin and thus improve resolution. To test this prediction, the number of overhanging layers was controlled by repositioning the channels in the z-direction (Fig. 5), using a layer height of 50 µm. Square channels that were printed near the base of the print, with 1.5 mm thick overhangs and thus 30 overhang layers, printed cleanly only down to 1.0 mm (Fig. 5B). Decreasing the overhang thickness to 0.5 mm (10 overhang layers) improved the resolution by ~0.2 mm (Fig. 5C), consistent with the prediction.

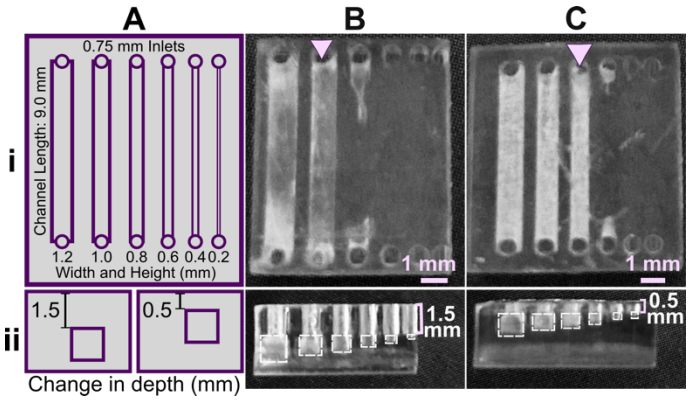

Fig.5. Reducing the number of overhang layers in the chip design improved the resolution of internal features. (**A**) Schematic of the test piece with six internal channels, in (**i**) top view and (**ii**) side view. (**B**,**C**) Channels were printed with (**B**) 1.5 mm or (**C**) 0.5 mm overhang thickness, and imaged from (**i**) top and (**ii**) side. The square channel is traced with dashed outlines; the features visible above the channel in the side view are inlets and outlets. All pieces were printed in FL Clear resin with a 405 nm light source (settings in Table S1). Resolution was determined visually by observing the smallest channel cross-section that could be printed fully (pink arrows).

An additional strategy to improve resin drainage from interior channels is to use shorter channels or add drainage pores, when feasible in the design. Especially with smaller cross sections (≤0.5 mm for the FL resin), channels were increasingly difficult to drain as the length of the internal channel increased (Fig. 6A). Should this kind of blockage be seen in a feature, draining pores potentially could be added. Indeed, in the viscous FL Clear resin, pores added to the channels in the test piece improved print resolution from 1 mm (Fig. 4B) to 0.6 mm (Fig. 6B); in this experiment, we arbitrarily added more pores to channels with smaller cross sections to ensure sufficient drainage. To minimize disruption of the channel, we found that it was best to use pores with a diameter the same or slightly smaller than the channel; smaller pores did not provide sufficient drainage and were filled with uncured resin (Fig. 6C). A potential concern with this method is that large open pores could cause leakage when the channel is filled with fluid. We have found that in low-pressure flow applications, surface-tension based pinning is sufficient to prevent leakage (data not shown). Should one wish to fill the holes, however, several options exist. We found that pinholes can be filled with uncured resin through capillary action and cured with UV light (data not shown), though care should be taken to not block the internal channels.

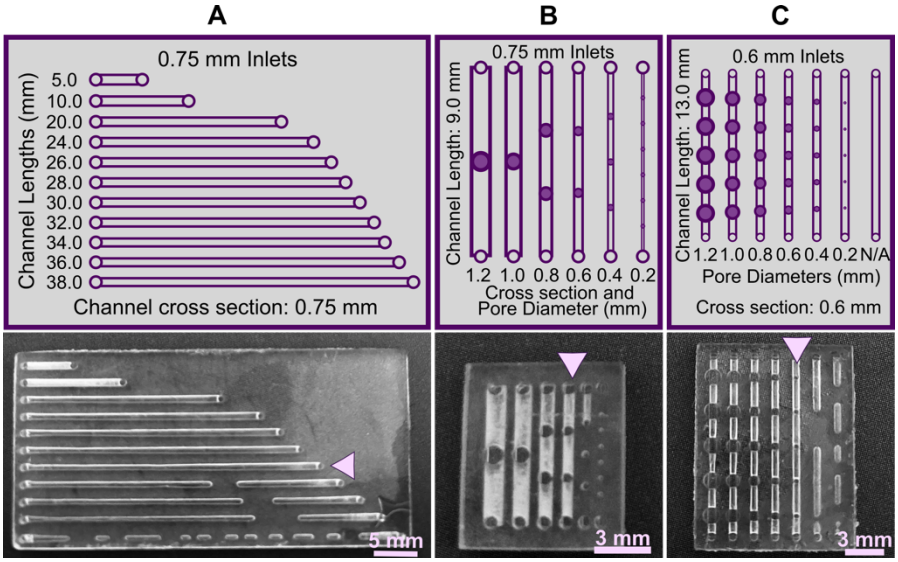

Fig. 6. Adding apertures of the same diameter or larger to an internal feature or decreasing channel length can improve resolution. All prints were with a 405 nm light source, 100 µm layer height, and FormLabs Clear resin. (**A)** Channels with fixed 0.75 mm cross sections and varied lengths from 5.0 – 38.0 mm. (**B)** An adaptation of the original test piece (**Fig. 3, 4**) with draining pores (filled purple circles) of the same width as each channel. (**C)** Varied pore sizes over a fixed channel cross section of 0.6 mmResolution was determined visually by observing how small of a channel cross-section can be printed clearly in each design (pink arrows).

3.4 Cytocompatibility of resins with primary cells

Cytocompatibility has been the most challenging issue for 3D printed parts used with live cultures and tissues. Many recent publications have addressed this issue, as noted in the introduction. Common solutions include coating the materials to reduce contact with cells or leaching them to extract many of the toxic substances,[22,30] or producing homemade resins with more biocompatible photoabsorbers.[25,60,61] Here, we tested an overnight, heat and saline leaching method that was straight-forward and required minimal manual steps. This approach was similar to previous leaching methods,[17,30] but was expediated from several days to a 24 hour timeframe by placing all pieces in PBS and leaching overnight near their maximum heat stability temperatures (Table 1). This accelerated timescale provided relatively quick turnaround times between fabrication and device application. To test cytocompatibility, we used primary, naïve murine splenocytes, a cell type that is more sensitive to small changes in their culture environment than some hardier immortalized cell lines.[62]

We found that for experiments under 4 hours, the overnight leaching treatment was sufficient to increase viability of primary murine splenocytes in contact with 3D printed materials (Fig. 7A). Splenocytes cultured in direct physical contact with either FL resin retained viability high enough (>60%) after 4 hr to enable short on chip experiments with the treated materials, whereas untreated materials resulted in lower viability on average. In contrast, while treating the MC Bv007a resin did improve viability over the non-treated resin, it was still largely cytotoxic for these cells at 4 hours. The higher cytotoxicity is consistent with the greater quantity of potentially toxic additives in Bv007a compared to other resins (10-15%, Table 1). Furthermore, Bv007a had lower heat stability and could not be leached at the same temperature as the FL resins without mechanical damage (Section 3.1). Therefore, for short experiments with primary cells in suspension, we conclude that the Biomed or Clear resins are more suitable than BV007a and should be pre-treated to minimize release of toxic components into the culture.

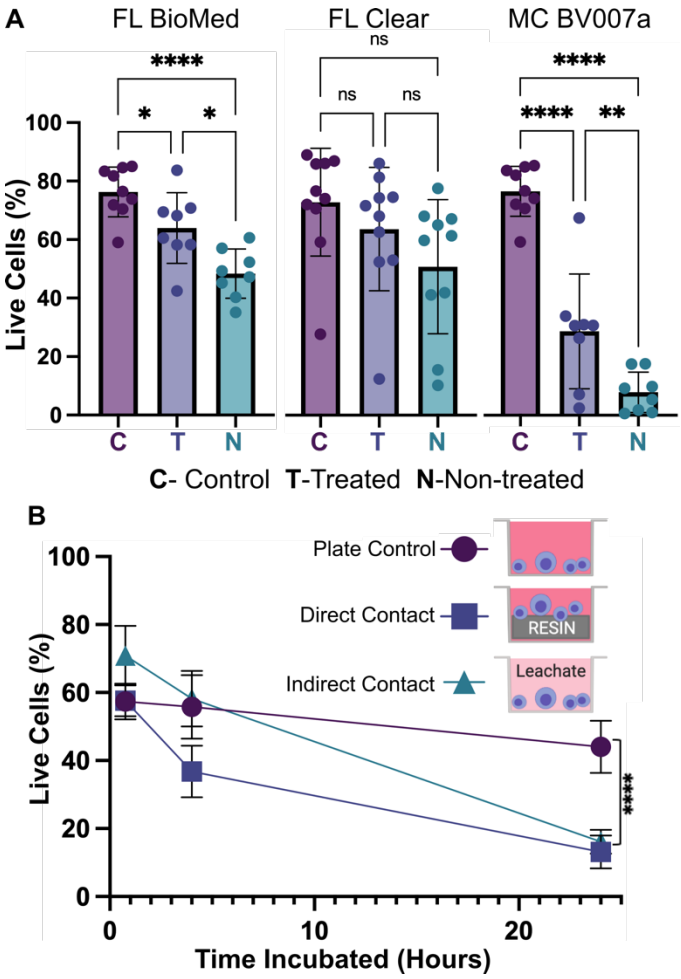

Fig. 7. Viability of primary murine splenocytes in contact with 3D printed materials. Primary splenocytes from male and female mice (N_{mice} = 2 per experiment) were evaluated by flow cytometry after live/dead staining with Calcein-AM/7AAD. (**A**) Cell viability after 4 hr of direct physical contact with PBS + heat treated (*T*) or non-treated (*N*) resins compared with well plate control (*C*). Treated BioMed and Clear prints maintained relatively high viability compared to the well plate, while Bv007 did not. (**B**) Viability of direct contact (i.e. culture with resin) and indirect contact (i.e. culture with resin leachate) of cells with treated BioMed prints at 45 min, 4 hours, and 24 hours showed a decrease in viability over time. Values show mean ± SD. Statistical analysis was performed using a one-way ANOVA at the final time point with ****$p < 0.0001$, **$p < 0.001$, and *$p < 0.01$.

As many experiments require longer term culture than just 4 hr, we finally tested splenocyte viability over time when cultured in direct physical contact with treated FL BioMed resin or in "indirect contact," i.e. cultured in contact with media that was pre-conditioned by incubation with the resin. Direct contact with resin is likely to occur in a fully integrated bioanalytical microchip with on-chip cell culture, while indirect contact may occur when microdevices are used to prepare materials used in cell culture (e.g.

mixers or droplet microfluidics) or to deliver media components to cultures (e.g. flow channels or bubble traps). We again found that viability was high for both contact conditions within 0-4 hr, but viability decreased overnight (24 hrs) for both contact conditions compared to plate controls (Fig. 7B). Others have reported longer culture times than this for hardier cell lines.[17,23,25,28–30,32,63,64] This result indicates that at least for primary murine splenocytes and perhaps for other fragile cells, more work is needed to identify best practices for post-print treatments and/or more biocompatible resin formulations.

3.5 Optical components of resins

Microfluidics is frequently integrated with on-chip imaging. Autofluorescence is a potential limitation of polymeric chips, whereas PDMS is often praised for its optical compatibility. Therefore, we quantified the autofluorescence of each of the representative resins in four standard fluorescence channels. In the Cy5 and Rhodamine channels, all three resins showed relatively low autofluorescence and were comparable to PDMS (Fig. 8). However, UV excitation (DAPI channel) elicited high levels of autofluorescence from the two FormLabs resins. The Clear resin also showed moderate autofluorescence in the GFP channel. Autofluorescence at short wavelengths is consistent with the use of photoabsorbers intended to absorb at short wavelengths.[60] On the other hand, MC Bv007a had negligible autofluorescence in all channels, similar to PDMS. Thus, optical compatibility in the intended fluorescence channels should inform material choice for microfluidics devices.

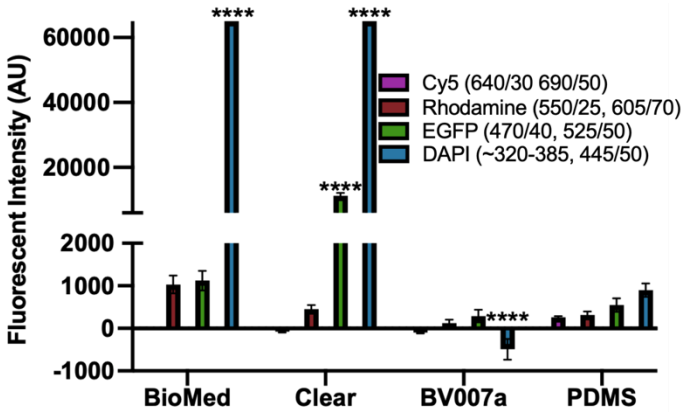

Fig.8. Autofluorescence depended on material composition and fluorescence filter set. BioMed, Clear, and BV007a prints were evaluated in comparison to PDMS for autofluorescence in Cy5, Rhodamine, EGFP, and DAPI fluorescent channels. Background subtracted mean grey values were analyzed with ImageJ and used to determine the fluorescent intensity of each material. Saturation values were at 65,000 AU. Bars show mean and standard deviation, N=3 intensity measurements per print. Two-way ANOVA, comparisons shown between resin results versus PDMS for each respective fluorescent channel, ****p<0.0001.

Optical clarity (transparency) is also important for microscopy and imaging. Various approaches for improving this property have been suggested in published papers as well as on vendor and hobbyist websites (r\3Dprinting, All3DP, etc.).[25,34] Here we compared 5 of these methods head to head, using the FL Clear resin as a base, to determine which would be best for increasing the transparency of a printed piece (Fig. 9). All methods were compared to a glass slide as a positive control. Pieces that were printed flush against the rough base plate (i.e. without the use of supports or rafts) came off the base plate slightly cloudy in appearance (Fig. 9VI). This cloudiness was intensified when attempting to buff both the base end and the vat end of the print with a typical nail file (Fig. 9VII). Since the nail file did not have a fine sanding grain, it ended up doing more harm than good by producing new scratches on the surface of the print.

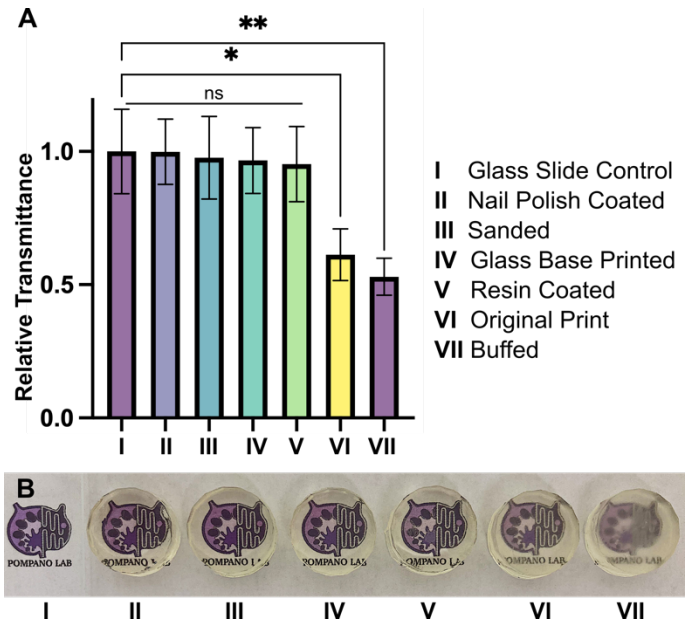

Fig.9. Optical clarity of clear resins was enhanced with post-treatments that achieved material transparency similar to glass. Round prints of FormLabs Clear resin were printed with the MiiCraft Ultra 50 405 printer and post-treated as listed in the legend, labels II -VII. (**A)** Transmittance was evaluated using an upright microscope. Relative transmittance was compared to the average light transmittance through a 0.17 mm thick glass slide (I). Bars show mean ± standard deviation, n = 3. One-way ANOVA, Tukey's post-hoc test; *p = 0.0284, **p = 0.0067, and ns > 0.05. (**B)** Photo of the test pieces laid over the Pompano Lab logo for qualitative, visual comparison (captured with phone camera).

Several methods proved successful in improving optical clarity. The quickest method that produced glass-like clarity was the nail polish coating of both the base and vat sides of the print (Fig. 9II). The nail polish only took a few seconds to apply and approximately 10 minutes to dry on each side, which introduced a challenge to keep dust out of the polish while drying on an open countertop. Sanding the piece with micron grain sandpaper avoided the issue of dust and the pieces emerged smooth (Fig. 9III) instead of scratched like the nail-filed ("buffed") piece (Fig. 9VII). Sanding the printed part on at least the baseplate-side is especially recommended if it will not disrupt any print features, as it more easily maintained a uniform surface than the other methods. Printing directly on glass[25] (Fig. 9IV) had similar impacts to sanding and is recommended for smaller prints that would be easier to remove from a glass slide. This approach requires some caution, though, as attaching glass to a baseplate can cause increased wear and tear to a printing vat. It also requires resetting the initial layer height so that the printer does not lower the baseplate too far into the vat. Resin coating (Fig. 9V) was also helpful for increasing transparency, but it

was difficult to achieve without overcuring the rest of the print or under-curing the additional coat, which was also prone to capturing dust. Relative to the glass slide control, most of the post-treated 3D prints were determined to have acceptable transparency. Although tested here for a single resin, we expect that these methods would have similar results on most semi-transparent or transparent SL resins.

4. Conclusion

In using 3D printing for production of microfluidic devices, compromises and strategic design choices are often required to best match the material and design to the required experiment. After identifying priorities based on the planned experiments, a resin should be chosen that best fits the requirements of print resolution, mechanical stability, cytocompatibility, and optical compatibility, informed by a foundational understanding of material components. If needed, printer settings and device designs can be modified to increase the integrity of printed parts and resolution of interior channels, and post-treatment methods can be used to increase the cytocompatibility and optical clarity of a printed piece. Print stability can be improved by reducing mechanical stress in the design of a piece, and internal feature resolution can be increased by ensuring adequate resin drainage and minimizing the photoexposure of trapped resin, e.g. by reducing the number of overhanging layers. Viability can be improved upon by leaching toxins out of prints prior to application with cells, though there is still a need for more biocompatible options, especially for sensitive primary cells. Optical clarity of parts printed with clear resins can be improved via polishing methods to achieve glass-like transparency. In the future, resins that are high-resolution, cytocompatible, and optically clear resins will certainly be an area of continued commercial development, and promising PEG-DA based resin formulas have been reported that can be made in-house.[25,60,61] Meanwhile, the considerations and best practices recorded here can help researchers begin to integrate SL 3D printing fabrication with commercially available products into their microfluidics research. We envision that this guide and its head-to-head comparison of conditions will help streamline the fabrication workflow for researchers who are new to 3D printing within the biomicrofluidic community.

Author contributions statement

H.B. Musgrove: Conceptualization, methodology, investigation, data curation, formal analysis, visualization, writing – original draft, review and editing **M.A. Catterton:** Conceptualization guidance, methodology, writing – review and editing **R.R. Pompano**: Funding acquisition, supervision, writing – review, editing, and finalization

Conflict of interest statement

The authors have no conflicting interests to declare.

Acknowledgements

Research reported in this publication was supported by the National Institute of Allergy and Infectious Diseases under Award No. R01AI131723 and from the National Institute of Biomedical Imaging and Bioengineering under Award No. R03EB028043 through the National Institute of Health (NIH). The content is solely the responsibility of the authors and does not necessarily represent the official views of the National Institutes of Health. The authors would like to thank Amirus Saleheen for his suggestions for post-treating resins in preparation for cell culture, Scott Karas for his assistance with sanding prints, Alexander Ball for his expertise and assistance with flow cytometry experiments, and Michael Ly for his correspondence regarding MiiCraft and CadWorks3D resins and printers.

References

(1) Morbioli, G. G.; Speller, N. C.; Stockton, A. M. A Practical Guide to Rapid-Prototyping of PDMS-Based Microfluidic Devices: A Tutorial. *Anal. Chim. Acta* **2020**, *1135*, 150–174. https://doi.org/10.1016/j.aca.2020.09.013.

(2) Torino, S.; Corrado, B.; Iodice, M.; Coppola, G. PDMS-Based Microfluidic Devices for Cell Culture. *Inventions* **2018**, *3* (3), 65. https://doi.org/10.3390/inventions3030065.

(3) Zhang, C.; Bills, B. J.; Manicke, N. E. Rapid Prototyping Using 3D Printing in Bioanalytical Research. *Bioanalysis* **2017**, *9* (4), 329–331. https://doi.org/10.4155/bio-2016-0293.

(4) Dirkzwager, R. M.; Liang, S.; Tanner, J. A. Development of Aptamer-Based Point-of-Care Diagnostic Devices for Malaria Using Three-Dimensional Printing Rapid Prototyping. *ACS Sens.* **2016**, *1* (4), 420–426. https://doi.org/10.1021/acssensors.5b00175.

(5) Bhattacharjee, N.; Urrios, A.; Kang, S.; Folch, A. The Upcoming 3D-Printing Revolution in Microfluidics. *Lab. Chip* **2016**, *16* (10), 1720–1742. https://doi.org/10.1039/C6LC00163G.

(6) Gale, B.; Jafek, A.; Lambert, C.; Goenner, B.; Moghimifam, H.; Nze, U.; Kamarapu, S. A Review of Current Methods in Microfluidic Device Fabrication and Future Commercialization Prospects. *Inventions* **2018**, *3* (3), 60. https://doi.org/10.3390/inventions3030060.

(7) Yazdi, A. A.; Popma, A.; Wong, W.; Nguyen, T.; Pan, Y.; Xu, J. 3D Printing: An Emerging Tool for Novel Microfluidics and Lab-on-a-Chip Applications. *Microfluid. Nanofluidics* **2016**, *20* (3), 50. https://doi.org/10.1007/s10404-016-1715-4.

(8) Nielsen, A. V.; Beauchamp, M. J.; Nordin, G. P.; Woolley, A. T. 3D Printed Microfluidics. *Annu. Rev. Anal. Chem.* **2020**, *13* (1), 45–65. https://doi.org/10.1146/annurev-anchem-091619-102649.

(9) SLA vs. DLP: Guide to Resin 3D Printers https://formlabs.com/blog/resin-3d-printer-comparison-sla-vs-dlp/ (accessed 2021 -08 -13).

(10) High-Accuracy 3D Printing Materials for Dental Labs and Practices https://dental.formlabs.com/materials/ (accessed 2020 -04 -27).

(11) Villanueva, D.; Haftka, R. T.; Sankar, B. V. Accounting for Future Redesign to Balance Performance and Development Costs. *Reliab. Eng. Syst. Saf.* **2014**, *124*, 56–67. https://doi.org/10.1016/j.ress.2013.11.013.

(12) Bishop, G. W.; Satterwhite-Warden, J. E.; Kadimisetty, K.; Rusling, J. F. 3D-Printed Bioanalytical Devices. *Nanotechnology* **2016**, *27* (28), 284002. https://doi.org/10.1088/0957-4484/27/28/284002.

(13) Chan, H. N.; Shu, Y.; Xiong, B.; Chen, Y.; Chen, Y.; Tian, Q.; Michael, S. A.; Shen, B.; Wu, H. Simple, Cost-Effective 3D Printed Microfluidic Components for Disposable, Point-of-Care Colorimetric Analysis. *ACS Sens.* **2016**, *1* (3), 227–234. https://doi.org/10.1021/acssensors.5b00100.

(14) Lambert, A.; Valiulis, S.; Cheng, Q. Advances in Optical Sensing and Bioanalysis Enabled by 3D Printing. *ACS Sens.* **2018**, *3* (12), 2475–2491. https://doi.org/10.1021/acssensors.8b01085.

(15) Ruan, X.; Wang, Y.; Cheng, N.; Niu, X.; Chang, Y.; Li, L.; Du, D.; Lin, Y. Emerging Applications of Additive Manufacturing in Biosensors and Bioanalytical Devices. *Adv. Mater. Technol.* **2020**, *5* (7), 2000171. https://doi.org/10.1002/admt.202000171.

(16) Meera Priyadarshini, B.; Dikshit, V.; Zhang, Y. 3D-Printed Bioreactors for In Vitro Modeling and Analysis. *Int. J. Bioprinting* **2020**, *6* (4). https://doi.org/10.18063/ijb.v6i4.267.

(17) Lembong, J.; Lerman, M. J.; Kingsbury, T. J.; Civin, C. I.; Fisher, J. P. A Fluidic Culture Platform for Spatially Patterned Cell Growth, Differentiation, and Cocultures. *Tissue Eng. Part A* **2018**, *24* (23–24), 1715–1732. https://doi.org/10.1089/ten.tea.2018.0020.

(18) Costa, P. F.; Albers, H. J.; Linssen, J. E. A.; Middelkamp, H. H. T.; van der Hout, L.; Passier, R.; van den Berg, A.; Malda, J.; van der Meer, A. D. Mimicking Arterial Thrombosis in a 3D-Printed Microfluidic in Vitro Vascular Model Based on Computed Tomography Angiography Data. *Lab. Chip* **2017**, *17* (16), 2785–2792. https://doi.org/10.1039/C7LC00202E.

(19) Brimmo, A.; Goyette, P.-A.; Alnemari, R.; Gervais, T.; Qasaimeh, M. A. 3D Printed Microfluidic Probes. *Sci. Rep.* **2018**, *8* (1), 10995. https://doi.org/10.1038/s41598-018-29304-x.

(20) de Almeida Monteiro Melo Ferraz, M.; Nagashima, J. B.; Venzac, B.; Le Gac, S.; Songsasen, N. A Dog Oviduct-on-a-Chip Model of Serous Tubal Intraepithelial Carcinoma. *Sci. Rep.* **2020**, *10* (1), 1575. https://doi.org/10.1038/s41598-020-58507-4.

(21) Shrestha, J.; Ghadiri, M.; Shanmugavel, M.; Razavi Bazaz, S.; Vasilescu, S.; Ding, L.; Ebrahimi Warkiani, M. A Rapidly Prototyped Lung-on-a-Chip Model Using 3D-Printed Molds. *Organs---Chip* **2019**, *1*, 100001. https://doi.org/10.1016/j.ooc.2020.100001.

(22) Kreß, S.; Schaller-Ammann, R.; Feiel, J.; Priedl, J.; Kasper, C.; Egger, D. 3D Printing of Cell Culture Devices: Assessment and Prevention of the Cytotoxicity of Photopolymers for Stereolithography. *Materials* **2020**, *13* (13), 3011. https://doi.org/10.3390/ma13133011.

(23) Carve, M.; Wlodkowic, D. 3D-Printed Chips: Compatibility of Additive Manufacturing Photopolymeric Substrata with Biological Applications. *Micromachines* **2018**, *9* (2), 91. https://doi.org/10.3390/mi9020091.

(24) Waheed, S.; Cabot, J. M.; Macdonald, N. P.; Lewis, T.; Guijt, R. M.; Paull, B.; Breadmore, M. C. 3D Printed Microfluidic Devices: Enablers and Barriers. *Lab. Chip* **2016**, *16* (11), 1993–2013. https://doi.org/10.1039/C6LC00284F.

(25) Urrios, A.; Parra-Cabrera, C.; Bhattacharjee, N.; Gonzalez-Suarez, A. M.; Rigat-Brugarolas, L. G.; Nallapatti, U.; Samitier, J.; DeForest, C. A.; Posas, F.; Garcia-Cordero, J. L.; Folch, A. 3D-Printing of Transparent Bio-Microfluidic Devices in PEG-DA. *Lab. Chip* **2016**, *16* (12), 2287–2294. https://doi.org/10.1039/C6LC00153J.

(26) Beauchamp, M.; Gong, H.; Woolley, A.; Nordin, G. 3D Printed Microfluidic Features Using Dose Control in X, Y, and Z Dimensions. *Micromachines* **2018**, *9* (7), 326. https://doi.org/10.3390/mi9070326.

(27) Michael J. Beauchamp. 3D Printed Microfluidic Devices for Bioanalysis, PhD Thesis, Brigham Young University, Utah, USA, July 7, 2019.

(28) Hart, C.; Didier, C. M.; Sommerhage, F.; Rajaraman, S. Biocompatibility of Blank, Post-Processed and Coated 3D Printed Resin Structures with Electrogenic Cells. *Biosensors* **2020**, *10* (11), 152. https://doi.org/10.3390/bios10110152.

(29) Sivashankar, S.; Agambayev, S.; Buttner, U.; Salama, K. N. Characterization of Solid UV Curable 3D Printer Resins for Biological Applications. In *2016 IEEE 11th Annual International Conference on Nano/Micro Engineered and Molecular Systems (NEMS)*; IEEE: Sendai, Japan, 2016; pp 305–309. https://doi.org/10.1109/NEMS.2016.7758255.

(30) Rimington, R. P.; Capel, A. J.; Player, D. J.; Bibb, R. J.; Christie, S. D. R.; Lewis, M. P. Feasibility and Biocompatibility of 3D-Printed Photopolymerized and Laser Sintered Polymers for Neuronal,

Myogenic, and Hepatic Cell Types. *Macromol. Biosci.* **2018**, *18* (7), 1800113. https://doi.org/10.1002/mabi.201800113.

(31) Gong, H.; Beauchamp, M.; Perry, S.; Woolley, A. T.; Nordin, G. P. Optical Approach to Resin Formulation for 3D Printed Microfluidics. *RSC Adv.* **2015**, *5* (129), 106621–106632. https://doi.org/10.1039/C5RA23855B.

(32) Carnero, B.; Bao-Varela, C.; Gómez-Varela, A. I.; Álvarez, E.; Flores-Arias, M. T. Microfluidic Devices Manufacturing with a Stereolithographic Printer for Biological Applications. *Mater. Sci. Eng. C* **2021**, *129*, 112388. https://doi.org/10.1016/j.msec.2021.112388.

(33) Ching, T.; Toh, Y.-C.; Hashimoto, M. Fabrication of Complex 3D Fluidic Networks via Modularized Stereolithography. *Adv. Eng. Mater.* **2020**, *22* (3), 1901109. https://doi.org/10.1002/adem.201901109.

(34) FormLabs. Guide to Clear 3D Printing https://formlabs.com/blog/3d-printing-transparent-parts-techniques-for-finishing-clear-resin/ (accessed 2021 -08 -13).

(35) Carrell, C. S.; McCord, C. P.; Wydallis, R. M.; Henry, C. S. Sealing 3D-Printed Parts to Poly(Dimethylsiloxane) for Simple Fabrication of Microfluidic Devices. *Anal. Chim. Acta* **2020**, *1124*, 78–84. https://doi.org/10.1016/j.aca.2020.05.014.

(36) Catterton, M. A.; Montalbine, A. N.; Pompano, R. R. Selective Fluorination of the Surface of Polymeric Materials after Stereolithography 3D Printing. *Langmuir* **2021**, *37* (24), 7341–7348. https://doi.org/10.1021/acs.langmuir.1c00625.

(37) FormLabs. Form Wash time settings https://support.formlabs.com/s/article/Form-Wash-Time-Settings?language=en_US (accessed 2021 -08 -13).

(38) Hart, C.; Didier, C. M.; Sommerhage, F.; Rajaraman, S. Biocompatibility of Blank, Post-Processed and Coated 3D Printed Resin Structures with Electrogenic Cells. *Biosensors* **2020**, *10* (11), 152. https://doi.org/10.3390/bios10110152.

(39) Ball, A. G.; Belanger, M. C.; Pompano, R. R. Detergent Wash Improves Vaccinated Lymph Node Handling Ex Vivo. *J. Immunol. Methods* **2021**, *489*, 112943. https://doi.org/10.1016/j.jim.2020.112943.

(40) FormLabs. Certifications and standards https://support.formlabs.com/s/article/Certifications-and-standards?language=en_US (accessed 2021 -09 -24).

(41) *BioMed Clear Resin*; MSDS No. FLBMCL01 [Online]; FormLabs, Somerville, MA, May 28, 2020. Available from FormLabs. https://formlabs.com/3d-printers/form-3/tech-specs/#data-sheets (accessed 11/15/21)

(42) *Clear Resin*; MSDS No. FLGPCL04 [Online]; FormLabs, Somerville, MA, November 22, 2019. Available from FormLabs. https://formlabs.com/3d-printers/form-3/tech-specs/#data-sheets (accessed 11/15/21)

(43) Michael Ly. Viscosities of MiiCraft Clear and Master Mold Resins. Personal communication, August 17, 2021.

(44) *BV-007 Acrylate Polymers*, MSDS, Young Optics Inc. Hsinchu, Taiwan, January 24, 2016.

(45) Yang, Y.; Zhou, Y.; Lin, X.; Yang, Q.; Yang, G. Printability of External and Internal Structures Based on Digital Light Processing 3D Printing Technique. *Pharmaceutics* **2020**, *12* (3), 207. https://doi.org/10.3390/pharmaceutics12030207.

(46) Williams, C. G.; Malik, A. N.; Kim, T. K.; Manson, P. N.; Elisseeff, J. H. Variable Cytocompatibility of Six Cell Lines with Photoinitiators Used for Polymerizing Hydrogels and Cell Encapsulation. *Biomaterials* **2005**, *26* (11), 1211–1218. https://doi.org/10.1016/j.biomaterials.2004.04.024.

(47) Yoshii, E. Cytotoxic Effects of Acrylates and Methacrylates:Relationships of Monomer Structures and Cytotoxicity. *John Wiley Sons Inc JBiomed Mater Res* **1997**, *37*, 517–524.

(48) Eljezi, T.; Pinta, P.; Richard, D.; Pinguet, J.; Chezal, J.-M.; Chagnon, M.-C.; Sautou, V.; Grimandi, G.; Moreau, E. In Vitro Cytotoxic Effects of DEHP-Alternative Plasticizers and Their Primary Metabolites on a L929 Cell Line. *Chemosphere* **2017**, *173*, 452–459. https://doi.org/10.1016/j.chemosphere.2017.01.026.

(49) Michael Ly. Humidity Recommendations for 3D Printing. Personal communication, November 2, 2021.

(50) Steyrer, B.; Busetti, B.; Harakály, G.; Liska, R.; Stampfl, J. Hot Lithography vs. Room Temperature DLP 3D-Printing of a Dimethacrylate. *Addit. Manuf.* **2018**, *21*, 209–214. https://doi.org/10.1016/j.addma.2018.03.013.

(51) FormLabs. Maintaining Resin Temperature https://support.formlabs.com/s/article/Maintaining-Resin-Temperature?language=en_US (accessed 2021 -11 -01).

(52) FormLabs. Cupping Blowout https://support.formlabs.com/s/article/Cupping-Blowout?language=en_US (accessed 2021 -09 -27).

(53) Obudho, B. How to Design Parts for SLA 3D Printing https://all3dp.com/2/how-to-design-parts-for-sla-3d-printing/ (accessed 2021 -10 -19).

(54) Markforged. Designing for Printing Part 2: Why 3D Printed Parts Warp and How to Stop It https://markforged.com/resources/blog/3d-printed-part-warping (accessed 2021 -10 -29).

(55) Schmidt, C.; Scherzer, T. Monitoring of the Shrinkage during the Photopolymerization of Acrylates Using Hyphenated Photorheometry/near-Infrared Spectroscopy. *J. Polym. Sci. Part B Polym. Phys.* **2015**, *53* (10), 729–739. https://doi.org/10.1002/polb.23694.

(56) Bagheri, A.; Jin, J. Photopolymerization in 3D Printing. *ACS Appl. Polym. Mater.* **2019**, *1* (4), 593–611. https://doi.org/10.1021/acsapm.8b00165.

(57) MacLean-Blevins, M. T. Preliminary Detailed Design. In *Designing Successful Products with Plastics*; Elsevier, 2018; pp 127–195. https://doi.org/10.1016/B978-0-323-44501-6.00006-4.

(58) Courtney Armstrong. How to design parts for SLA 3D printing https://www.hubs.com/knowledge-base/how-design-parts-sla-3d-printing/ (accessed 2021 -10 -25).

(59) FormLabs. Adjusting layer thickness in PreForm https://support.formlabs.com/s/article/When-to-Use-Different-Layer-Heights?language=en_US (accessed 2021 -08 -31).

(60) Gong, H.; Bickham, B. P.; Woolley, A. T.; Nordin, G. P. Custom 3D Printer and Resin for 18 Mm × 20 Mm Microfluidic Flow Channels. *Lab. Chip* **2017**, *17* (17), 2899–2909. https://doi.org/10.1039/C7LC00644F.

(61) Warr, C.; Valdoz, J. C.; Bickham, B. P.; Knight, C. J.; Franks, N. A.; Chartrand, N.; Van Ry, P. M.; Christensen, K. A.; Nordin, G. P.; Cook, A. D. Biocompatible PEGDA Resin for 3D Printing. *ACS Appl. Bio Mater.* **2020**, *3* (4), 2239–2244. https://doi.org/10.1021/acsabm.0c00055.

(62) Butler, M. *Animal Cell Culture and Technology*; The basics; IRL Press at Oxford University Press: Oxford ; New York, 1996.

(63) Chang, S.; Popowich, Y.; Greco, R. S.; Haimovich, B. Neutrophil Survival on Biomaterials Is Determined by Surface Topography. *J. Vasc. Surg.* **2003**, *37* (5), 1082–1090. https://doi.org/10.1067/mva.2003.160.

(64) Takenaga, S.; Schneider, B.; Erbay, E.; Biselli, M.; Schnitzler, Th.; Schöning, M. J.; Wagner, T. Fabrication of Biocompatible Lab-on-Chip Devices for Biomedical Applications by Means of a 3D-Printing Process: Fabrication of Biocompatible Lab-on-Chip Devices for Biomedical Applications. *Phys. Status Solidi A* **2015**, *212* (6), 1347–1352. https://doi.org/10.1002/pssa.201532053.